Finite-Element Analysis of Slow-Wave Schottky Contact Printed Lines

CHING-KUANG TZUANG, STUDENT MEMBER, IEEE, AND TATSUO ITOH, FELLOW, IEEE

Abstract—**Extensive finite-element analyses on MMIC slow-wave structures with both localized and layered models are presented. Good agreement is achieved between the data presented here and other theoretical results and experiments. Higher order elements that improve accuracy are discussed. The comparative studies for Schottky contact microstrip and coplanar waveguide with localized and layered models are presented. Potential applications of the localized models to more general and practical slow-wave circuits are also discussed.**

I. Introduction

THE ADVANCE in monolithic microwave integrated circuits (MMIC's) has led to widespread applications of microstrip and other planar transmission lines such as coplanar waveguide (CPW) and coupled microstrip on semiconductor substrate. In addition to interconnection or transmission-line applications, this class of transmission lines can be employed as circuit elements such as phase shifters, voltage-tunable filters, and voltage-controlled attenuators [1]–[3].

These applications are made possible by the slow-wave propagation resulting from electron–electromagnetic interaction with the lossy semiconductor material. The device was experimentally studied with metal–insulator–semiconductor (MIS) configurations and with Schottky contact microstrip or CPW structures [3]–[6] and was theoretically investigated by a number of techniques, such as spectral-domain analysis (SDA), the mode-matching method, and the finite-element method (FEM) [7]–[10] based on MIS or so-called layered models. However, practical semiconductor devices such as Schottky contact microstrip or CPW are certainly not laminated structures. Instead, they both have localized depletion regions on semiconductors. The effects of these localized depletion regions have never been discussed. It is plausible to contemplate that the layered model commonly used for the analysis may not correctly describe the actual field distributions in the structure with localized depletion regions.

In this paper, the finite-element method based on the $E_z - H_z$ formulation [9], [11] is used for a variety of slow-wave structures which can best be described by the localized model. In conjunction with this study, use of higher order elements, e.g., quadratic isoparametric elements, is discussed and its results are presented.

Manuscript received April 1, 1986; revised June 25, 1986. This work was supported in part by Grant AFOSR-86-0036.

The authors are with the Department of Electrical and Computer Engineering, University of Texas at Austin, Austin, TX 78712.

IEEE Log Number 8610550.

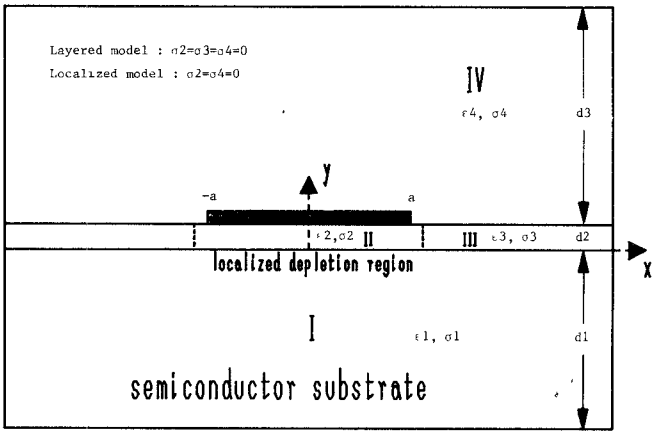

Fig. 1. Localized depletion model for Schottky contact *microstrip*.

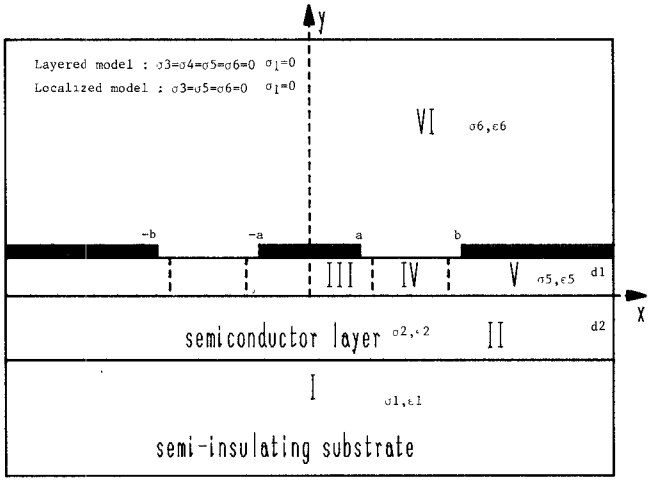

Fig. 2. Localized depletion model for Schottky contact *coplanar waveguide*.

II. Localized Models

The localized depletion models for Schottky contact microstrip and CPW are illustrated in Figs. 1 and 2, respectively. By setting the conductivity in region III of Fig. 1 and that in region IV of Fig. 2 to zero, the localized models will be reduced to the conventional MIS or layered models.

Obviously, the boundaries of the depletion region in actual devices are not straight lines but are curved. Such curved boundaries can be found from solutions of a static Poisson's equation for a given bias condition. The present algorithm can then be applied to such geometry. However,

0018-9480/86/1200-1483$01.00 ©

the objective of the present paper is to study the effect of localization. The essential feature can be found without solving the structures with curved depletion boundaries. Therefore, the localized depletion region is assumed to be rectangular in shape.

Furthermore, we are also interested in the development of low-loss slow-wave circuit elements. Schottky contacts for both center and ground strips of the CPW are assumed under the same dc bias conditions. It is found that the loss in this CPW structure can be less than the case where only the center conductor is a Schottky contact in the CPW.

III. Derivation of the Matrix Equation

A. Theory

The conventional $E_z - H_z$ formulation that results in a homogeneous coupled symmetric matrix equation is adopted in this paper [9], [11]. In the lossless case, the finite-element method with the $E_z - H_z$ formulation provides a variational solution. The matrix equation can be derived by a functional followed by the Ritz approximation [11] or by weighted residual integration followed by the Galerkin's method [9]. It is possible to obtain a variational statement of the problem even for lossy structure by dividing E_z and H_z components into real and imaginary parts [12]. Alternatively, the three-vector H formulation can be used [13], [14]. This includes mixed boundary conditions, and caution must be exercised in treating the singularity at the corner of conductor edge. The conventional $E_z - H_z$ formulation used here does not provide a variational solution for the lossy system. The method used here forces the residual to be zero by making it orthogonal to each member of a complete set of the trial functions. This method is one manifestation of the method of weighted residuals, which does not require the existence of a variational principle [15], [16]. Not only is the method of weighted residuals simple for implementation; in principle, a systematic improvement in the accuracy of solution can be obtained if enough terms of the trial functions are used. Section IV-B discusses such improvements if one chooses quadratic elements instead of bilinear elements in the lossy waveguide system.

For purposes of clarity, a brief description of the derived $E_z - H_z$ formulation is shown in the Appendix.

B. Application of the Finite-Element Method

The important steps for the actual coding of the final matrix equation obtained can be found in [17]. The hierarchy of the program can accept any isoparametric elements. In the present paper, we use four-node bilinear and quadratic eight-node elements. Their differences in terms of numerical results will be discussed.

By alternating E_z and H_z nodal variables in the column vector X, the matrix A becomes a banded matrix (Appendix). Finally, rows and columns corresponding to the Dirichlet boundary conditions are deleted such that E_z and H_z vanish at electric and magnetic walls, respectively. Therefore, the matrix A has dimension $N \times N$, where N equals $(2M - L)$. M is the total number of nodes and L stands for the sum of the total number of nodes located on electric or magnetic walls. The complex root of the equation, $\det(A) = 0$, is the solution for the propagation constant. The real and imaginary parts of the propagation constant correspond to the attenuation constant and slow-wave factor, respectively.

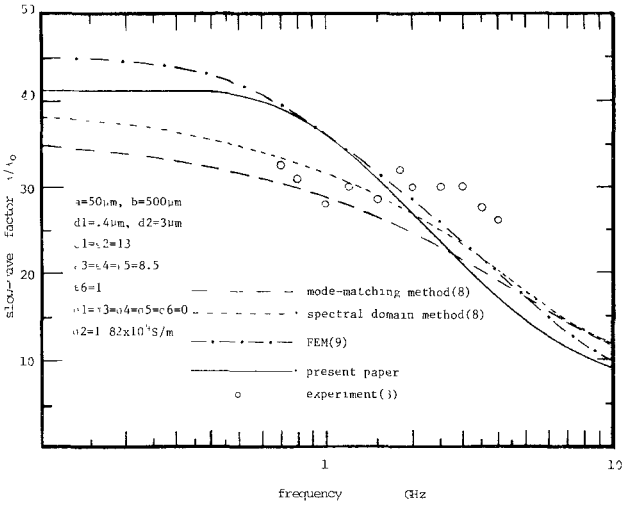

Fig. 3. Plots of *slow-wave factor* as obtained by the present paper and other theories such as mode-matching method [8], SDA [8], and FEM [9] together with experimental data [3] for an MIS CPW.

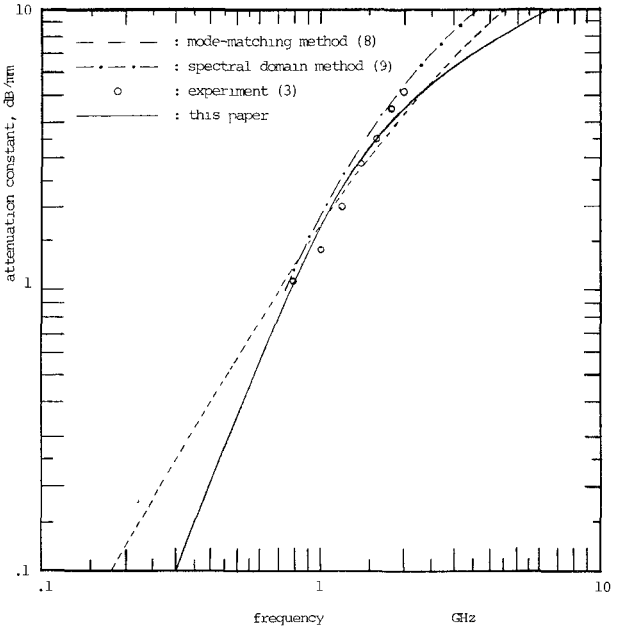

Fig. 4. Plots of *attenuation constant* as obtained by the present paper and other theories such as mode-matching method [8], SDA [9], and FEM [9] together with experimental data [3] for an MIS CPW.

IV. Numerical Results

A. Validity Check

The present FEM code is applied to lossless printed line structures, and excellent agreement has been obtained with the available data, such as [18, fig. 2.7 and fig. 7.11]. For the lossy layered case, Figs. 3 and 4 compare the results

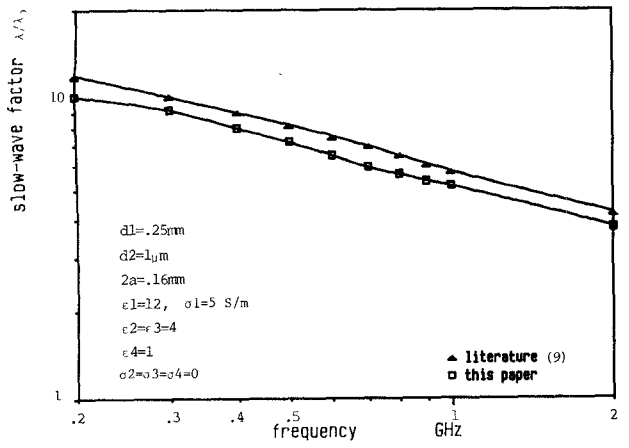

Fig. 5. Validity check of the results obtained by this paper and data in literature [9]; *slow-wave factor* versus frequency.

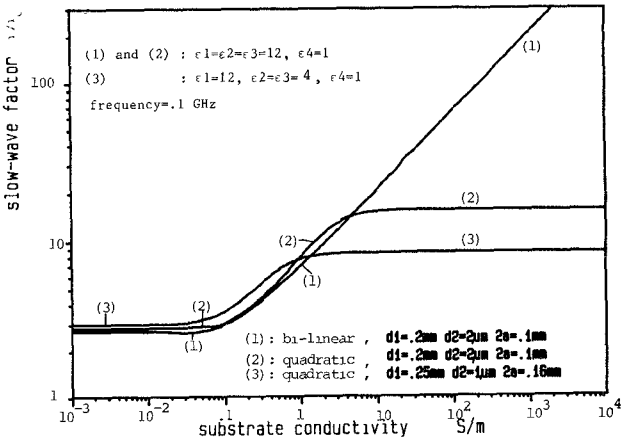

Fig. 7. Comparison of numerical results, *slow-wave factor* versus microstrip substrate conductivity, based on *quadratic and bilinear elements*.

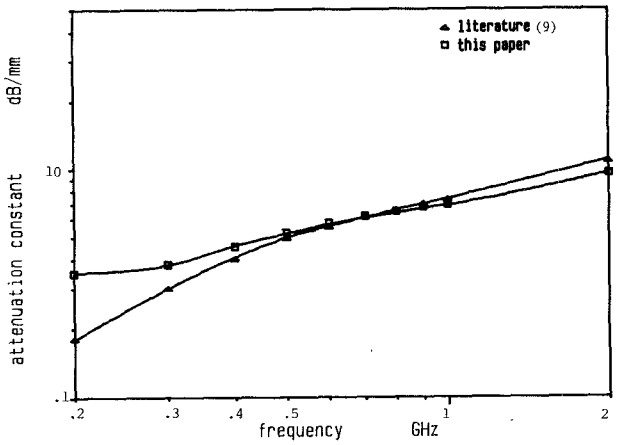

Fig. 6. Validity check of the results obtained by this paper and data in literature [9]; *attenuation constant* versus frequency.

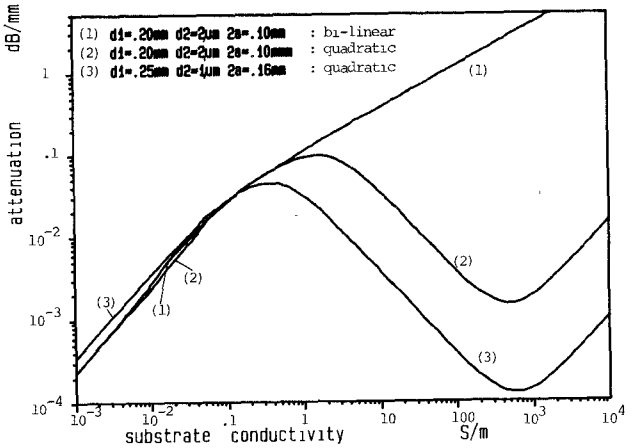

Fig. 8. Comparison of numerical results, *attenuation constant* versus microstrip substrate conductivity, based on *quadratic and bilinear elements*.

obtained by the present method as applied to the layered structure and other existing data for MIS CPW slow-wave propagation both theoretically and experimentally. The small discrepancy among various methods may be attributed to the CPW structure, which has a relatively high aspect ratio (b/a), i.e., 10, and a very thin insulating region. This makes it difficult to find very accurate answers over the frequency span of interest. In particular, it is well known that the slender element may yield poor results in FEM [19]. Owing to the fact that both the depletion and the lossy semiconductor regions are extremely thin, it is inevitable that slender elements exist if we do not use higher order and finer elements. Therefore, we apply quadratic eight-node elements, and a total of 96 nodes are employed for this particular structure.

The case for MIS microstrip slow-wave propagation is shown in Figs. 5 and 6, where the discretization based on bilinear elements and a total of 36 nodes are sufficient to match the data.

B. Bilinear Versus Quadratic Elements

Figs. 7 and 8 compare computational results for slow-wave propagation in an MIS microstrip model based on both bilinear and quadratic elements. Both the slow-wave factor and the attenuation constant agree very well in low substrate conductivity, say, less than 0.1 S/m.

When bilinear elements are used, the slow-wave factor and the attenuation constant approach infinity as substrate conductivity increases. Clearly this is nonphysical because very high conducting substrate can be regarded as a metal layer and the slow-wave factor should be brought down when the substrate turns into metal. In fact, in the case of quadratic elements, the slow-wave factor starts to decline gradually and loss starts to increase again when substrate conductivity is increased from approximately 500 S/m. Similar comparative studies are performed for CPW localized model. We also obtain similar phenomena in that both the slow-wave factor and the attenuation constant approach infinity when we employ bilinear elements and increase substrate conductivity.

Another type of comparative study is performed, i.e., numerical computations of the slow-wave factor and attenuation constant versus frequency by applying both bilinear and quadratic elements on the same CPW structure. The results are illustrated in Figs. 9 and 10. In these figures, curves based on quadratic elements are identical to

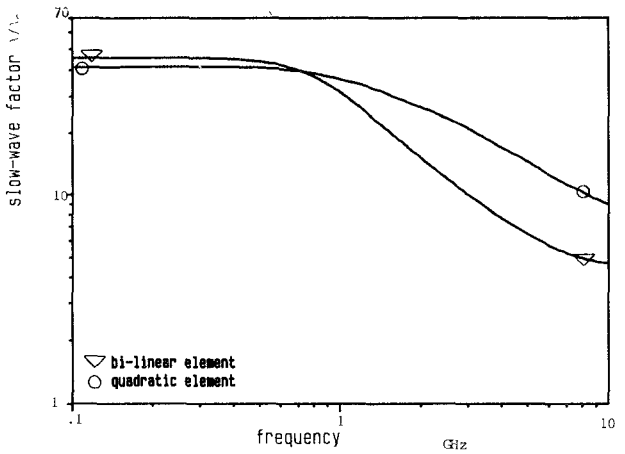

Fig. 9. Comparison of numerical results, *slow-wave factor* versus frequency, on the same MIS CPW structure analyzed in Figs. 3 and 4 based on *quadratic and bilinear elements*.

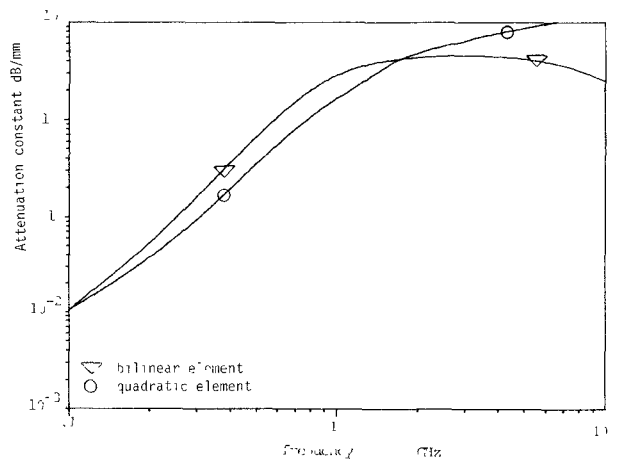

Fig. 10. Comparison of numerical results, *attenuation constant* versus frequency, on the same MIS CPW structure analyzed in Figs. 3 and 4 based on *quadratic and bilinear elements*.

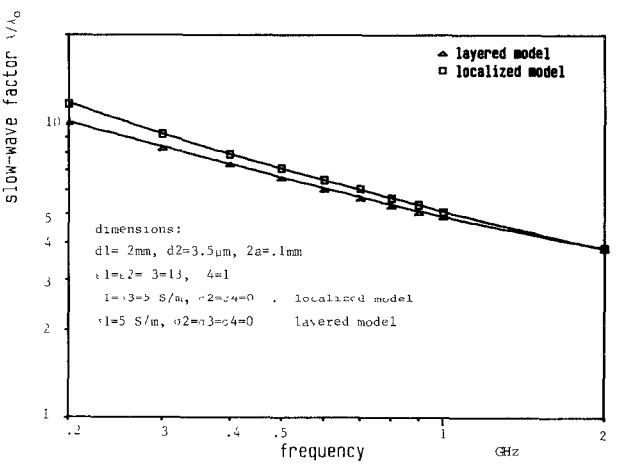

Fig 11. Comparisons of plots of *slow-wave factor* versus frequency based on *localized and layered* models for Schottky contact microstrips.

those used in Figs. 3 and 4. The solutions obtained by means of quadratic elements are apparently much closer to those obtained by other theoretical methods and experiments. Additional studies on MIS microstrip also draw the same conclusion.

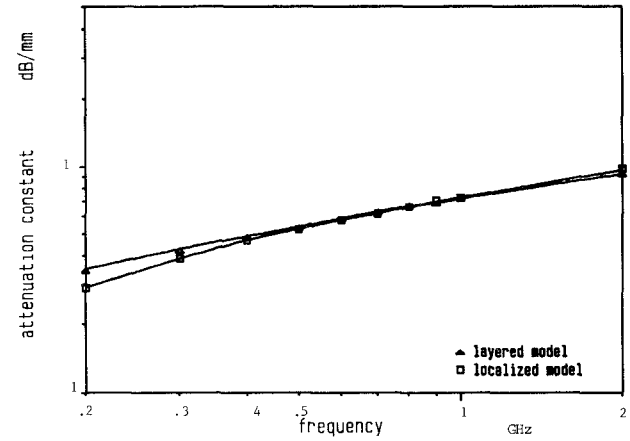

Fig. 12. Comparison of plots of *attenuation constant* versus frequency based on *localized and layered* models for Schottky contact microstrips.

TABLE I
COMPARISON OF SLOW-WAVE PROPAGATION FOR LAYERED AND LOCALIZED MICROSTRIP MODELS

	(slow-wave factor, dB/mm)		
MODEL	σ1(S/m) / σ3(S/m)	5	20×10^3
Layered	0	(8.364661, .0072815)	(8.397601, .0019445)
Localized	5	(8.391247, .0073026)	(8.397601, .0019502)
	20×10^3	(8.398345, .0067541)	(8.399383, .0019613)

Conditions: $a = 80\ \mu$m, d1 = 250 μm, d2 = 1 μm, $\epsilon1 = 12$, $\epsilon2 = \epsilon3 = 4$, $\epsilon4 = 1$, $\sigma2 = \sigma4 = 0$ (microstrip). Frequency = 0 1 GHz.

Since the accuracy of employing the quadratic elements in our particular application is confirmed, the rest of the computations in the paper are based on quadratic elements, except the results shown in Figs. 11 and 12.

C. Effects of Localized Depletion Regions on Slow-Wave Propagation

It is clear in Figs. 11 and 12 that the MIS layered model is a good model for *microstrip* slow-wave propagation. This conclusion is confirmed again by using quadratic elements with improved accuracy. The solutions obtained by layered and localized models are very close and cannot be distinguished by plots. Table I shows how close the solutions are under different combinations of conductivities. For the localized CPW model, the results shown in Figs. 13 and 14 are rather interesting. Structure (2) has about half the gap width of structure (1), and all the rest of the conditions are almost the same. The conducting region IV has a stronger influence on structure (2). A noticeable transition region exists where loss starts to decline and the slow-wave factor starts to change abruptly but settles quickly as σ_4 increases. The skin depth, which is inversely proportional to the square root of the conductivity, is relatively large in region IV, approximately 50 mm when σ_4 equals 0.1 S/m. The electromagnetic field penetrates region IV freely and interacts with it in terms of lossy dielectric material. When σ_4 is increased, say, to 10^5 S/m, the skin depth is reduced to 50 μm. This is very close to

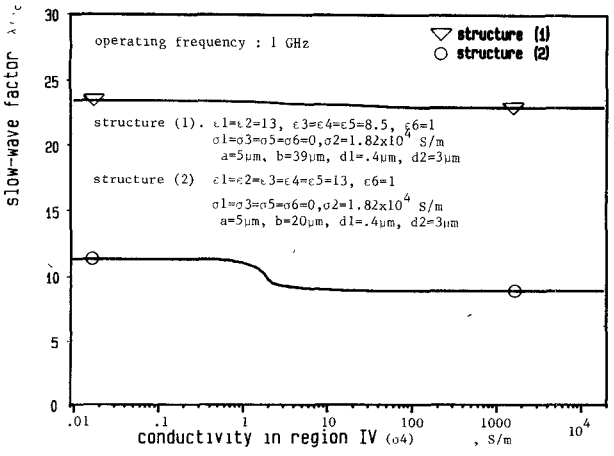

Fig. 13. Effects of *localized* depletion regions on CPW's; slow-wave factor versus conductivity of region IV in Fig. 2.

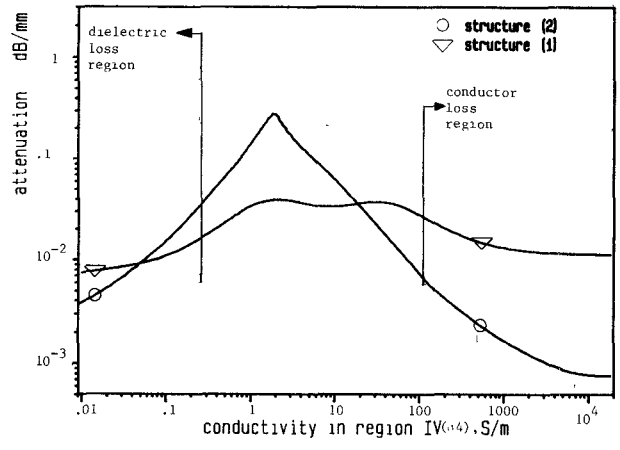

Fig. 14. Effects of *localized* depletion regions on CPW's; attenuation constant versus conductivity of region IV in Fig. 2.

the gap widths in structures (1) and (2). As a result, the highly conducting region IV can in effect be replaced by a piece of thin and imperfect metal inserted into the gap. The loss introduced at higher values of σ_4 is much more closely related to skin-effect ohmic loss. Generally speaking, we may separate the loss mechanism due to region IV in the structure into dielectric loss and conductor loss. The former increases as conductivity increases, and the latter decreases as conductivity increases. Common waveguides and transmission lines also exhibit similar loss behavior [20].

The qualitative discussions can be readily extended to obtain an equivalent transmission-line circuit representation of the localized CPW in Fig. 15. This empirical model happens to be a slight modification of the analytical model of the Schottky contact coplanar line based on semiempirical considerations and is indeed identical if we combine C_1 and C_3 into a single capacitor. Note that in our localized CPW structure, semiconductor Schottky contacts are under the metal strips. L_0 and R_0 represent the inductance and resistance due to ohmic loss and skin loss per unit length, respectively. C_0 represents the capacitance per unit length between center and ground strips in region VI. C_1 represents the capacitance per unit length from the

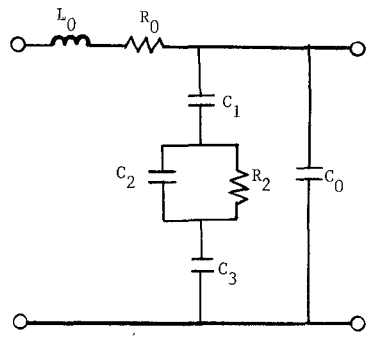

Fig. 15. Approximate transmission-line circuit representation of the Schottky contact CPW with localized depletion regions under metal strips.

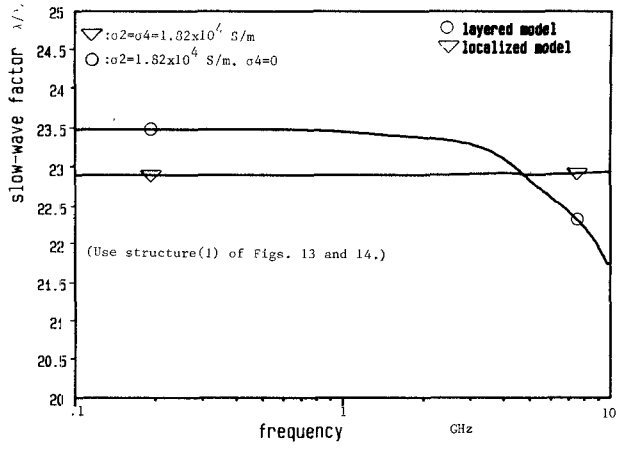

Fig. 16. Comparison of plots of *slow-wave factor* versus frequency based on localized and layered models for CPW's.

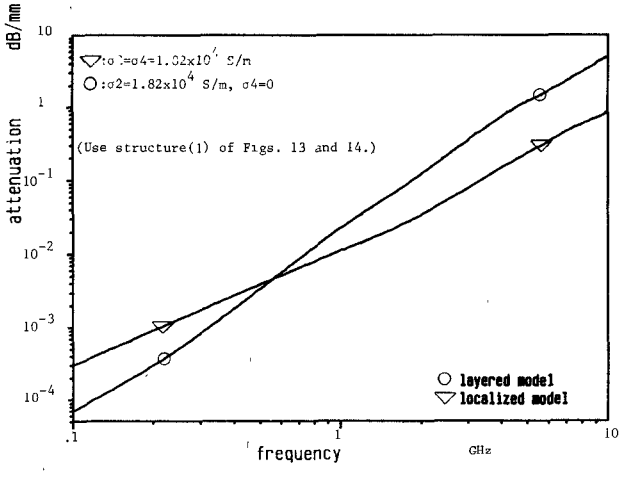

Fig. 17. Comparison of plots of *attenuation constant* versus frequency based on localized and layered models for CPW's.

center strip to the edges of region IV and region II. C_3 represents the capacitance per unit length from the ground strip to the other side of region IV and the edge of region II. Parallel R_2 and C_2 represent the circuit contribution of region IV and part of region II. General discussions leading to the determination of these component values can be found in [21] and [22].

Figs. 16 and 17 compare numerical results obtained by layered and localized models for slow-wave propagation on CPW's. The localized model tends to show better

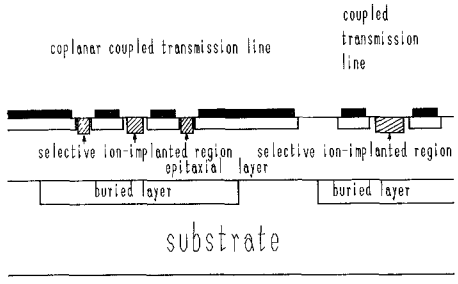

Fig. 18. Potential applications of the extensions of the localized models to MMIC planar waveguide designs, e.g., coupled coplanar lines and coupled lines with selective ion implantations, which add more degrees of freedom to design slow-wave circuits.

performance, with more linear slow-wave characteristics versus frequency and less loss at higher frequency in the structure under analysis. It suggests that the structure with Schottky contacts for all metal strips (Fig. 2) may become a practical slow-wave configuration.

V. Applications

Along with the study of the effects of the localized depletion models on MMIC slow-wave circuits, a general-purpose FEM program is developed for the analysis and design of planar waveguides. Fig. 18 shows several possible applications among a broad class of MMIC waveguides that can be analyzed by extensions of the present code. These structures cannot be modeled accurately by the MIS layered model. The results we obtained from the analyses of CPW and microstrip MMIC's with localized models suggest that we may tune the slow-wave circuit to meet certain design specifications by selective ion implantations on the locations proposed in Fig. 18, with appropriate controls over doping concentration and geometry. A certain mode of propagation may be more subject to the existing selective ion-implanted regions than another mode of propagation, and the additional ion-implanted region can enhance or reduce the loss associated with it depending on what the doping profile is.

VI. Conclusions

Extensive computer simulations employing FEM on CPW and microstrip MMIC slow-wave structures are performed to study the differences in slow-wave propagations between the layered model commonly used in the past and the localized model which is closer to physical situations. The results show that the layered model is a good approximation for the microstrip case. On the other hand, the localized model yields more accurate solutions for Schottky CPW. It is also pointed out that higher order elements improve solutions for the geometry under analysis. The work can be extended to analyze and design more complicated planar waveguides.

Appendix

In the homogeneous, isotropic, linear waveguide with uniform cross section, the Maxwell's equation can be represented by

$$\left(\nabla_t - \gamma \vec{U}_z\right) \times \left(\vec{E}_t + \vec{E}_z\right) = -j\omega\mu_{re}\mu_0\left(\vec{H}_t + \vec{H}_z\right) \quad (1)$$

$$\left(\nabla_t - \gamma \vec{U}_z\right) \times \left(\vec{H}_t + \vec{H}_z\right) = j\omega\epsilon_{re}\epsilon_0\left(\vec{E}_t + \vec{E}_z\right). \quad (2)$$

Note the following.

1) $e^{j\omega t}$ and $e^{-\gamma z}$ factors are assumed for a wave propagating along the positive z direction.

2) $\vec{E} = \vec{E}_t + \vec{E}_z$, $\vec{H} = \vec{H}_t + \vec{H}_z$; $\vec{E}_z = E_z\vec{U}_z$, $\vec{H}_z = H_z\vec{U}_z$. $\vec{U}_x$, $\vec{U}_y$, and $\vec{U}_z$ are unit vectors along the x, y, and z directions, respectively.

3) $\nabla_t = \vec{U}_x\partial/\partial x + \vec{U}_y\partial/\partial y$.

4) μ_0 and ϵ_0 are, respectively, the free-space permeability and permittivity, while μ_{re} and ϵ_{re} are the relative permeability and relative dielectric constant, respectively. Subscript e denotes *element number e* associated with subdomain Ω_e of the entire waveguide cross section region Ω, which contains N_e subdomains.

By defining the inner product as $(\vec{R}, \vec{S}) = \int_{\Omega_e} \vec{R}\cdot\vec{S}\,dx\,dy$ and test functions $\vec{P} = P\vec{U}_z$ and $P = 0$ on the magnetic wall and $\vec{Q} = Q\vec{U}_z$ and $Q = 0$ on the electric wall, one obtains

$$\sum_{e=1}^{N_e}\left(\vec{E}_t, \nabla_t \times \vec{P}\right) = \sum_{e=1}^{N_e} -j\omega\mu_{re}\mu_0\left(\vec{H}_z, \vec{P}\right) \quad (3)$$

$$\sum_{e=1}^{N_e}\left(\vec{H}_t, \nabla_t \times \vec{Q}\right) = \sum_{e=1}^{N_e} +j\omega\epsilon_{re}\epsilon_0\left(\vec{E}_z, \vec{Q}\right) \quad (4)$$

satisfying all the necessary boundary conditions.

Now we can derive expressions for $\vec{H}_t$ and $\vec{E}_t$ from (1) and (2) and substitute these into (3) and (4) to eliminate variables $\vec{H}_t$ and $\vec{E}_t$. To obtain an FEM representation of the boundary-value problem, we set

$$U = \sum_{j=1}^{M} u_j W_j^m$$

$$V = \sum_{j=1}^{M} v_j W_j^e$$

where W_j^m and W_j^e are shape functions at the jth node. M is the total number of nodes. Here, we use normalized variables $U = \sqrt{\mu_0}H_z$ and $V = \sqrt{\epsilon_0}E_z$. Note that $u_r = 0$ if the rth node is on the magnetic wall and $v_s = 0$ if the sth node is on the electric wall.

Next, we expand P and Q in terms of shape function W_i^m and W_i^e:

$$P = \sum_{j=1}^{M} p_i W_i^m$$

$$Q = \sum_{j=1}^{M} q_i W_i^e$$

where $W_i^m(x_r, y_r) = 0$ for $i = 1, M$ if the rth node is on the magnetic wall, and $W_i^e(x_s, y_s) = 0$ for $i = 1, M$ if the sth

node is on the electric wall

$$A = \begin{bmatrix} K^1_{M\times M} & K^2_{M\times M} \\ K^3_{M\times M} & K^4_{M\times M} \end{bmatrix}$$

$$K^1 = \int_\Omega \left\{ \mu_{re} \nabla_t W_i^m \cdot \nabla_t W_j^m / K_e^2 - \mu_{re} W_i^m W_j^m \right\} dx\,dy \quad (5)$$

$$K^4 = \int_\Omega \left\{ \epsilon_{re} \nabla_t W_i^e \cdot \nabla_t W_j^e / K_e^2 - \epsilon_{re} W_i^e W_j^e \right\} dx\,dy \quad (6)$$

$$K^2 = \int_\Omega \left\{ + j\gamma C \nabla_t W_i^m \times \nabla_t W_j^e / \omega K_e^2 \right\} dx\,dy \quad (7)$$

$$K^3 = \int_\Omega \left\{ - j\gamma C \nabla_t W_i^e \times \nabla_t W_j^m / \omega K_e^2 \right\} dx\,dy \quad (8)$$

where $K_e^2 = k_0^2 \mu_{re} \epsilon_{re} + \gamma^2$, $k_0 = 2\pi/\lambda_0$, and C = the velocity of light.

It can be shown that the matrix A is symmetric. The rows and columns corresponding to the nodes on magnetic walls and electric walls are deleted. Before the final assembly of the matrix A, the node variables are alternated and the column vector X has elements arranged in the following way: $u_1, v_1, u_2, v_2, \cdots$, etc. This results in a banded matrix A for saving computer storage.

References

[1] K. Frike and H. L. Hartnagel, "GaAs MESFET optimization and new device applications based on wave property studies," in *IEEE MTT-S Int. Microwave Symp. Dig.*, June 1985, pp. 192–195.

[2] C. Seguinot, P. Kennis, P. Pribetich, and J. F. Legier, "Performances prediction of an ultra broad-band voltage-controlled attenuator using Schottky contact coplanar line properties," *IEEE Electron Device Lett.*, vol. EDL-7, Feb. 1986.

[3] H. Hasegawa and H. Okizaki, "M.I.S. and Schottky slow-wave coplanar stripline on GaAs substrates," *Electron. Lett.*, vol. 13, pp. 663–664, Oct. 1977.

[4] H. Hasegawa, M. Furukawa, and H. Yanai, "Properties of microstriplines on Si–SiO_2 system," *IEEE Trans. Microwave Theory Tech.*, vol. MTT-19, pp. 869–881, Nov. 1971.

[5] D. Jager, "Slow-wave propagation along variable Schottky-contact microstrip line," *IEEE Trans. Microwave Theory Tech.*, vol. MTT-24, pp. 566–573, Sept. 1976.

[6] D. Jager and W. Rabus, "Bias dependent phase delay of Schottky-contact microstrip line," *Electron Lett.*, vol. 9, no. 9, pp. 201–203, 1973.

[7] Y. C. Shih and T. Itoh, "Analysis of printed transmission lines for monolithic integrated circuits," *Electron. Lett.*, vol. 18, no. 14, pp. 585–586, July 1982.

[8] Y. Fukuoka, Y. C. Shih, and T. Itoh, "Analysis of slow-wave coplanar waveguide for monolithic integrated circuits," *IEEE Trans. Microwave Theory Tech.*, vol. MTT-31, pp. 567–573, July 1983.

[9] M. Aubourg, J. P. Villotte, F. Goon, and Y. Grault, "Analysis of M.I.S. or Schottky contact coplanar lines using the F.E.M. and S.D.A.," in *IEEE MTT-S Int. Microwave Symp. Dig.*, June 1983, pp. 396–398.

[10] R. Sorrentino, G. Leuzzi, and A. Silbermann, "Characteristics of metal–insulator–semiconductor coplanar waveguides for monolithic microwave circuits," *IEEE Trans. Microwave Theory Tech.*, vol. MTT-32, pp. 410–416, Apr. 1984.

[11] P. Daly, "Hybrid-mode analysis of microstrip by finite element methods," *IEEE Trans. Microwave Theory Tech.*, vol. MTT-19, pp. 19–25, Jan. 1971.

[12] A. D. McAulay, "Variational finite-element solution for dissipative waveguides and transportation application," *IEEE Trans. Microwave Theory Tech.*, vol. MTT-25, pp. 382–392, May 1977.

[13] S. R. Cvetkovic and J. B. Davies, "Self-adjoint vector variational formulation for lossy anisotropic dielectric waveguide," *IEEE Trans. Microwave Theory Tech.*, vol. MTT-34, pp. 129–134, Jan. 1986.

[14] C. H. Chen and C. Lien, "The variational principle for non-self-adjoint electromagnetic problems," *IEEE Trans. Microwave Theory Tech.*, vol. MTT-28, pp. 878–886, Aug. 1980.

[15] A. K. Noor, "Multifield (mixed and hybrid) finite element model," in *State-of-the-Art Surveys on Finite Element Technology*, 1983, ch. 5, pp. 127–156.

[16] B. A. Finlayson, *The Method of Weighted Residuals and Variational Principles*. New York: Academic Press, 1972.

[17] E. B. Becker, G. F. Carey, and J. T. Oden, *Finite Elements*, vol. I. Englewood Cliffs, NJ: Prentice-Hall, 1981.

[18] K. C. Gupta, R. Garg, and I. J. Bahl, *Microstrip Lines and Slot Lines*. Dedham, MA: Artech House, 1979.

[19] G. F. Carey and J. T. Oden, *Finite Elements*, vol. II. Englewood Cliffs, NJ: Prentice-Hall, 1983.

[20] S. Ramo, J. R. Whinnery, and T. V. Duzer, *Fields and Waves in Communication Electronics*. New York: Wiley, 1965.

[21] C. Seguinot, P. Kennis, P. Pribetich, and J. F. Legier, "Analytical model of the Schottky contact coplanar line," in *Proc. 14th European Microwave Conf.*, Sept. 1984, pp. 160–165.

[22] H. Hasegawa and S. Seki, "Analysis of interconnection delay on very high-speed LSI/VLSI chips using an MIS microstrip line model," *IEEE Trans. Microwave Theory Tech.*, vol. MTT-32, pp. 1721–1727, Dec. 1984.

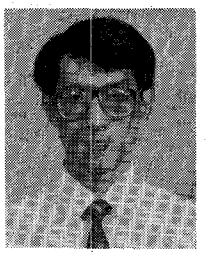

Ching-Kuang Tzuang (S'84) was born in Taiwan, Republic of China, on May 10, 1955. He received the B.S. degree in electronics engineering from National Chiao Tung University, Hsin Chu, Taiwan, in 1977 and the M.S. degree in electrical engineering from the University of California at Los Angeles in 1980.

From February 1981 to June 1984, he was employed at TRW, Redondo Beach, CA, working on high-speed and microwave integrated circuits. He is currently a research assistant studying toward the Ph.D. degree at the University of Texas at Austin. His current research interest is in monolithic microwave integrated circuits and components.

Tatsuo Itoh (S'69–M'69–SM'74–F'82) received the Ph.D. degree in electrical engineering from the University of Illinois, Urbana, in 1969.

From September 1966 to April 1976, he was with the Electrical Engineering Department, University of Illinois. From April 1976 to August 1977, he was a Senior Research Engineer in the Radio Physics Laboratory, SRI International, Menlo Park, CA. From August 1977 to June 1978, he was an Associate Professor at the University of Kentucky, Lexington. In July 1978, he joined the faculty at the University of Texas at Austin, where he is now a Professor of Electrical and Computer Engineering and Director of the Electrical Engineering Research Laboratory. During the summer 1979, he was a guest researcher at AEG-Telefunken, Ulm, Germany. Since September 1983, he has held the Hayden Head Centennial Professorship of Engineering at the University of Texas. Since September 1984, he has been Associate Chairman for Research and Planning of the Electrical and Computer Engineering Department.

Dr. Itoh is a member of the Institute of Electronics and Communication Engineers of Japan, Sigma Xi, and Commission B of USNC/URSI. He served as the Editor of IEEE TRANSACTIONS ON MICROWAVE THEORY AND TECHNIQUES for 1983–1985. He serves on the Administrative Committee of IEEE Microwave Theory and Techniques Society. He is a Professional Engineer registered in the state of Texas.